Appl. Phys. B (2017) 123:78
DOI 10.1007/s00340-017-6663-5

Applied Physics B
Lasers and Optics

RAPID COMMUNICATION

Quasi-4D laser diagnostics using an acousto-optic deflector scanning system

Tao Li[1] · Jhon Pareja[1,2] · Lukas Becker[1] · Wolfgang Heddrich[3] · Andreas Dreizler[1,2] · Benjamin Böhm[4]

Received: 10 October 2016 / Accepted: 7 February 2017 / Published online: 3 March 2017

Abstract In this paper, a novel scanning system for laser diagnostics was developed and characterized. The system is based on the acousto-optic deflection of a high-speed pulsed laser. Results showed that quasi-volumetric laser illumination with high precision and accuracy can be achieved with a simplified and flexible optical setup. The feasibility of the method for performing high-speed quasi-4D laser diagnostics was demonstrated by the tomographic visualization of a lifted turbulent jet flame using Mie-scattering and multi-plane particle image velocimetry measurements of a turbulent non-reactive mixing case. Three-dimensional flame and flow structures can be detected and tracked with this new scanning system.

1 Introduction

Two-dimensional laser measurement techniques such as particle image velocimetry (PIV) and planar laser-induced fluorescence (PLIF) have been widely used in combustion diagnostics [1]. However, these methods suffer from deficient out-of-plane information which limits the understanding of complex three-dimensional transient events. Particularly, in turbulent flames and ignition events out-of-plane motion plays an important role [2]. Therefore, spatially and temporally resolved measurements are essential for a deeper understanding of flame-flow interactions.

In recent years, many efforts have been made towards obtaining spatially resolved experimental data in combustion studies. Multiple laser sheets, including crossed- and parallel-plane measurements of OH-PLIF combined with normal [3] or stereoscopic PIV [4, 5] have been used to produce quasi four-dimensional (4D) information during experiments with turbulent flames. Volumetric imaging employing volumetric laser illumination and multiple cameras for the detection has been applied for tomographic measurements of the velocity field [6–8] and flame chemiluminescence [9].

By sweeping a laser sheet fast enough across the measurement volume, quasi three-dimensional (3D) measurements can be achieved. These techniques can be divided in two groups: oscillating mirrors (e.g., galvanometric scanners and stepper motors) [10, 11] and polygonal mirrors [12, 14]. Although they are proved to be effective for tracking transient events in combustion and fluid dynamics applications, their maximal scan frequency is restricted by the inertia related to the moving mechanical parts [12]. The high inertia is an additional safety issue which needs to be considered.

An alternative to mirror-based mechanical deflection is the optical solid state deflection by means of an acousto-optic deflector (AOD) [15]. With an AOD, a light beam can be deflected by inducing a high-frequency acoustic wave through a crystal to change its refractive index periodically. The frequency of the acoustic wave can be varied to

✉ Benjamin Böhm
bboehm@ekt.tu-darmstadt.de

[1] Reaktive Strömungen und Messtechnik, Technische Universität Darmstadt, Jovanka-Bontschits-Straße 2, 64287 Darmstadt, Germany

[2] Darmstadt Graduate School of Excellence Energy Science and Engineering, Technische Universität Darmstadt, Jovanka-Bontschits-Straße 2, 64287 Darmstadt, Germany

[3] Fachbereich Mathematik und Naturwissenschaften, Hochschule Darmstadt, Schöfferstraße 3, 64285 Darmstadt, Germany

[4] Energie- und Kraftwerkstechnik, Technische Universität Darmstadt, Jovanka-Bontschits-Straße 2, 64287 Darmstadt, Germany

deflect the beam at different angles. Then, if the frequency is continuously varied, the light beam can be scanned over a range of deflection angles. Because the deflection angle is adjusted by the voltage, any position within the maximum scan range can be approached by a voltage curve. This allows individually adjusting the distance between single laser positions and flexibly varying scan parameters even during ongoing experiments. This is advantageous when compared to polygonal mirrors, where the mirror geometry needs to be optimized for each application. AODs have been used in microscopy, optical storage and laser-material processing where high speed controlled deflection of the light beam is desired [15]. However, to the best of the authors' knowledge, there are no studies in the literature applying AODs to combustion diagnostics.

This paper introduces a novel method applying an acousto-optic deflector to perform high-speed quasi-4D laser diagnostics without any mechanical moving parts. The characterization of the scanning system configuration using a high-speed pulsed laser was carried out in terms of laser position fluctuation, scanning frequency, parallelization, spatial resolution, and scan depth. The capabilities of the system are demonstrated through the quasi-4D visualization of a lifted turbulent jet flame using Mie-scattering of oil droplets and time series multi-plane PIV measurements of a turbulent non-reactive mixing case. Finally, the AOD scanning approach is compared with a polygonal laser scanning mirror.

2 Materials and methods

2.1 Acousto-optic beam deflection

As schematically shown in Fig. 1, the AOD system is mainly composed of a crystal, a piezoelectric transducer, a radio frequency (RF) driver and a DC source. If operated at a certain input voltage, the driver applies a RF signal to the piezoelectric-transducer producing a high-frequency acoustic wave which propagates through the crystal. When the incident beam interacts with the acoustic wave, the crystal works like an optical diffracting grating and the output beam will be deflected in different diffraction orders. If the AOD is designed to operate in the Bragg regime [16], at one particular incident angle, θ_B, only one diffraction order is produced (first order beam) although a fraction of the beam is still transmitted through the crystal (zero order beam). The ratio between the energy of the beam diffracted into the first order and the energy of the incident beam can be defined as the diffraction efficiency. In practice, AODs can reach diffraction efficiencies up to 90% [17]. Under the Bragg regime and an isotropic interaction (i.e., the acoustic wave travels longitudinally in the crystal and the incident

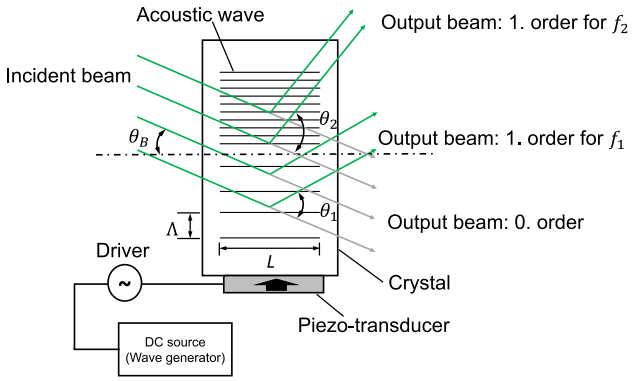

Fig. 1 Acousto-optic deflector system and light deflection in the Bragg regime with acoustic frequency variation. θ_1 and θ_2 illustrate two different deflection angles of the 1. order for two different acoustic frequencies f_1 and f_2

and diffracted laser beams experience the same refractive index), the angle of the incident light must be adjusted to the so-called Bragg angle, θ_B

$$\sin\theta_B = \frac{\lambda}{2\Lambda} = \frac{\lambda f}{2v} \tag{1}$$

where Λ is the acoustic wavelength, λ is the optical wavelength inside the crystal, and f is the frequency of the acoustic wave traveling at the velocity v inside the crystal. The following boundary condition must be satisfied

$$L \gg \frac{\Lambda^2}{\lambda} \tag{2}$$

where L is the interaction length, which is the distance the laser beam travels through the acoustic wave. The separation angle between the first order and zero order beams, θ, is twice the Bragg angle. For a certain light wavelength and a certain material, the separation angle is determined only by f. As illustrated in Fig. 1 for two different acoustic frequencies (f_1 and f_2), if $f_1 < f_2$, the corresponding separation angle $\theta_1 < \theta_2$. Therefore, the periodic variation of the acoustic frequency can be used to vary the deflection angle as basis of a laser scanning technique using an AOD. $\Delta\theta = \theta_2 - \theta_1$ is defined here as the scan angle range.

2.2 Acousto-optic deflector (AOD) scanning system with a high-speed pulsed laser

The experimental setup of the scanning system is schematically shown in Fig. 2. The AOD (see Fig. 1) consisted of an 1-axis deflector for 532 nm (AA Opto-Electronic, DTSX-400-532, TeO_2 crystal). The damage threshold is 2.5 W/mm^2 (average power) for 532 nm and the diffraction efficiency is above 80% for the entire scan angle range. This AOD was combined with a voltage controlled oscillator (VCO) driver (AA Opto-Electronic, DFA10Y-B-0-50.110).

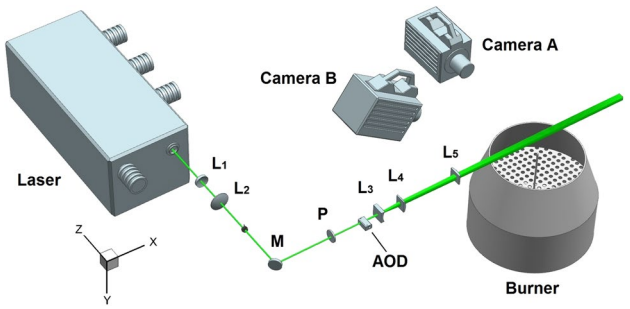

Fig. 2 Experimental setup of the scanning system for the tomographic imaging of a lifted flame and multi-plane PIV of a turbulent non-reactive mixing case

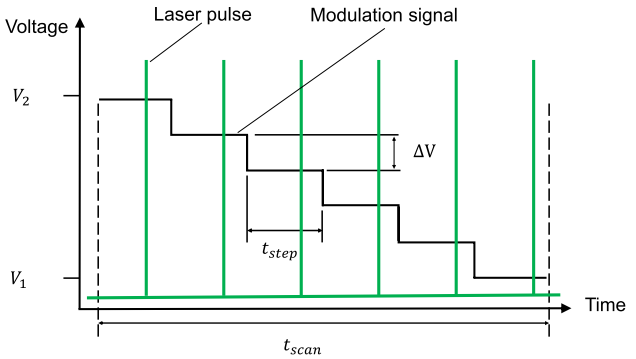

Fig. 3 Synchronization of the step function modulation signal and a pulsed laser for a scan with scan angle range, $V_2 - V_1$, and scan frequency, $f_{\text{scan}} = 1/t_{\text{scan}}$. Modulation signal divided into several steps, ΔV, with duration, t_{step}

The driver required an input voltage between 0 and 10 V to sweep the acoustic frequency between 55 and 105 MHz, producing a maximum scan angle range, $\Delta\theta_{\text{max}} = \theta_{10\text{V}} - \theta_{0\text{V}} = 2.35°$. An amplifier (AA Opto-Electronic, AMPA-B-30) was used to provide the necessary RF power to drive the AOD device up to 1 W. A two-channel arbitrary waveform generator (Keysight Technologies, 33522B) supplied user-defined voltage signals to control the VCO driver, and therefore the scanning parameters such as deflection direction, scan frequency and scan angle range. A frequency-doubled high-speed dual-cavity Nd:YVO_4 laser (Edgewave IS411-DE, 9 ns pulse length, 0.5 mJ/pulse, maximum repetition rate 30 kHz/cavity) was used as a light source. The diameter of the laser beam was adapted to the optical aperture of the AOD (7.5×7.5 mm) using two spherical lenses ($L_1, f_1 = -100$ mm and L_2, $f_2 = +150$ mm in Fig. 2) thus avoiding any crystal damage. One advantage of the AOD scanning system, when performing laser diagnostics, is that only one cylindrical lens (L_5, $f_5 = +400$ mm in Fig. 2) is necessary to simultaneously parallelize and focus at the measurement volume the multiple laser beams from different deflection angles.

2.3 Laser beam position control

Referring to Eq. (1), the deflection angle of the light beam is determined by the acoustic frequency which depends linearly on the input voltage signal given to the VCO driver. Thus, the beam position and movement can be easily controlled by modulating the input voltage signal. To scan the angle between two positions, the input voltage signal (thus the acoustic frequency) needs to be scanned. The beam movement will respond accordingly to the scan frequency, velocity and range with which the input voltage of the driver is modulated. However, a continuous increase or decrease of the acoustic frequency causes a deformation of the beam, which is known as cylinder-lensing effect [18]. This is related to the access time, which is the time the acoustic wave takes to cross the laser beam, and therefore, the time it takes the beam to respond to a change in input voltage signal. The access time of the AOD was 10.3 μs for a beam diameter of 6.7 mm. The response time can be decreased by reducing the beam diameter, while any crystal damage should be avoided.

In this work, an innovative method was implemented to scan the separation angle while avoiding the cylinder-lensing effect with a pulsed laser. As schematically represented in Fig. 3, instead of continuously varying the input voltage, the signal was modulated with a step function. The modulation signal between V_2 and V_1 with a duration, t_{scan}, and scan frequency, $f_{\text{scan}} = 1/t_{\text{scan}}$, was divided into several steps, ΔV, with equal duration, t_{step}. ΔV determines the number of angular positions in which the scan range ($V_2 - V_1$) is separated (i.e., the spatial resolution in the scan direction). Because in this case a pulsed laser was used, the modulation signal and the laser pulses were temporally synchronized so that when a laser pulse crossed the crystal, an acoustic wave of constant frequency was propagating through it. This required a t_{step} longer than the access time. Thereby, the diffraction was uniform and no optical compensation was necessary.

2.4 Demonstration experiments: flame front detection and multi-plane PIV

The capabilities of the scanning system were evaluated through two demonstration experiments: a quasi-4D visualization of a lifted turbulent jet flame and time series multi-plane PIV measurements of a turbulent non-reactive mixing case.

Referring again to Fig. 2, a non-premixed burner provided a lifted turbulent methane jet flame. The burner consists of a fuel lance of 8 mm inner diameter and 350 mm length, surrounded by an air co-flow of 130 mm inner

diameter. The fuel lance was long enough to provide fully developed pipe flow at the exit and it was tapered to a sharp edge to minimize recirculation. The bulk exit velocity of the jet and co-flow were 10 and 0.2 m/s, respectively. The calculated Reynolds number of jet was ~5000. Under these operating conditions, the flame had a lift-off height of ~ 28 mm [9].

The flame front was detected by means of Mie-scattering. Both flows, the jet and co-flow were seeded with silicon oil droplets with a mean diameter of ~1 μm, using two seeders (AGF 10.0 Palas). Planar illumination of the seeded droplets at the flame base was achieved by including a telescope in the setup with two cylindrical lens (L_3, $f_3 = -50$ mm and L_4,$f_4 = +150$ mm in Fig. 2). In combination with L_5, a laser sheet of 24 mm height and 300 μm thickness was formed at the measurement location (i.e., the lifted flame base). Quasi-volumetric illumination of the oil droplets was achieved by scanning the laser sheet in the z-axis direction using the AOD scanning system.

The laser was operated using both cavities in an equidistant alternating fire mode to obtain a repetition rate of 60 kHz. The laser beams were overlapped by a polarizing beam splitter. Because the polarization of the cavities is perpendicular to each other and the AOD diffraction efficiency depends on the polarization of the incident light, the difference in polarization from both beams resulted in an enormous difference in diffracted laser energy. To overcome this, a lambda half-wave plate (P in Fig. 2) was mounted before the AOD to rotate the polarization of both beams to an angle, at which, the same diffraction efficiency (around 40%) was obtained for both cavities.

Different scanning parameters were evaluated for the flame front detection, which are summarized in Table 1. Two scan depths (z-axis) of 6.3 and 13.7 mm were defined, with the current optical setup, by modulating the input voltage signal between 9.5 and 5.5 V and between 9.5 and 1.5 V, respectively. The scan frequency, f_{scan} was varied from 2 to 20 kHz. Because the laser repetition rate was fixed to 60 kHz, each f_{scan} yielded a defined number of laser sheets, N_s, with a defined separation distance, Δz. For all conditions t_{step} was 16.5 μs.

Table 1 Scan parameters for flame front detection experiments

Scan depth (mm)	f_{scan} (kHz)	N_S	Δz (mm)
6.3	2	30	0.21
	5	12	0.53
	10	6	1.05
	20	3	2.10
13.7	2	30	0.46
	5	12	1.14
	10	6	2.28
	20	3	4.57

f_{scan} represents the scan frequency, N_s is the number of laser sheets and Δz is the separation distance between laser sheets

The resulting Mie-scattering signals from the multiple measurement planes were collected perpendicularly to the xy-plane and imaged onto a single CMOS camera (LaVision GmbH, HSS6), see camera A in Fig. 2. The frame rate of the camera was synchronized with the laser repetition rate and the exposure time was set to 16 μs. For the 6.3 mm scan depth, the camera was equipped with a 85 mm lens (NIKKOR, f# = 5.6) while for the 13.7 mm case, a 60 mm lens (NIKKOR AF Micro, f# = 5.6) was employed. Another CMOS camera (LaVision, HSS6) was mounted parallel to the x-axis and above the scanner (camera B in Fig. 2) and equipped with a 105 mm lens (SIGMA Macro lens, f# = 5.6) to determine the parallelization of the multiple laser sheets in the x-axis direction. For this purpose and prior to the measurements, a ceramic plate was placed at the burner nozzle, orthogonally to the laser sheets. The laser sheets were scanned and the diffuse light reflected at each laser sheet position was collected by camera B. The ceramic plate and the camera were translated along the x-axis using a traversing unit and the measurements were repeated at several positions to reconstruct the paths of the laser sheets.

The Mie-scattering images were recorded using the software Davis (LaVision, Version 8.3.0). Images of a calibration target (LaVision, Type 7) were recorded at the location of each laser sheet in the measurement volume. For flame detection, a high seeding density was used. When the seeded oil droplets reached the flame, they were evaporated. Therefore, the Mie-scattering signal was present only in unburnt gas regions, which was exploited to mark the flame contour. In this way, the recorded raw images were first corrected by the intensity inhomogeneities of the laser sheet. Then, a local standard deviation filter and a 3×3 px median filter were applied to compensate the inhomogeneous seeding in the image. Finally, the filtered images were binarized to distinguish the burnt and unburnt regions.

In the case of the multi-plane PIV demonstration experiment, the burner was operated without igniting the flame to provide a non-reactive turbulent mixing problem. The seeding density was optimized for PIV and the laser was operated with a single cavity at 30 kHz. The lambda half-wave plate was rotated to optimize the diffraction efficiency and increase the Mie-scattering signal necessary for PIV. Using the same optical setup as for the flame detection experiment, the scanning parameters were adjusted to generate three laser sheet planes with a constant $\Delta z = 0.75$ mm at $f_{scan} = 5$ kHz. The measurement volume (scan depth of 1.5 mm) was located at the center axis of the jet. Based on the bulk velocity range of the jet and co-flow, the time-series PIV approach was sufficient for measuring the

velocity fields with a single laser cavity. In this sense, the t_{step} of the modulation signal was adjusted to allow two consecutive laser shots ($\Delta t = 33.33\,\mu s$, $t_{step} = 66\,\mu s$) at each of the three measurement planes. The camera was equipped with a 100 mm lens (Carl Zeiss, f# = 8) to capture the signal from all measurement planes. Images processing and velocity field calculations were performed with the software Davis (LaVision, Version 8.3.0).

3 Results

Alignment and parallelization of the laser sheets through the measurement volume have a strong influence on the accuracy of any measurement performed with the scanning system. Figure 4 illustrates an example result of the parallelization of the laser sheets, in terms of the laser path along the x-axis, for a scan depth of 6.3 mm at $f_{scan} = 5$ kHz. The averaged position of 12 laser sheets were measured along 40 mm with 2 mm increments in the x-axis direction using 200 individual scans. The parallelization and uniformity of the paths is evident. The maximum deviation of the averaged position along the measured paths was 60 μm, which represents a deviation angle of 0.086°. In the case of the measurement volume with 13.7 mm scan depth, the maximum deviation was 100 μm or 0.14°. Moreover, in the measurement volume of the lifted flame experiment (marked by the two vertical dashed lines in Fig. 4) the deviations of the laser sheet paths were even smaller. To evaluate the precision of the scanning system, additional measurements of the fluctuations of the laser sheet position along the z-axis were performed for different scan frequencies using a lateral effect photodiode (Thorlabs, PDP90A), similarly to Ref. [12]. Results showed that the spatial jitter of the position of the laser sheets during scanning was in the order of the laser jitter (standard deviation of the laser beam position was ~9 μm) for all scanning parameter tested.

Figure 5 presents a snapshot of the volumetric reconstruction of the lifted flame base from 30 two-dimensional images recorded at a scan frequency of 2 kHz. The portion of the flame base displayed corresponds to a scan volume of 13.7 mm depth and it is represented here as the isosurface of the location of the evaporation of seeding droplets at the unburnt/burnt gases layer. The main dimensions, asymmetry and 3D features of the flame base are comparable to those of previous experiments [9, 12]. The integral length scale at the flame base was estimated to be ~2 mm. The integral time scale was ~4 ms as estimated from the integral length scale and mean velocity at the flame base. A detailed discussion on the time and length scales is provided in Ref. [12]. The Kolmogorov time scale was estimated to be in the order of 60 μs. The laser scan duration of 0.5 ms was approximately 1/8th of the integral time scale and eight times larger than the Kolmogorov time scale. Therefore, the largest scales are expected to be well resolved in the quasi-4D measurements while the smallest scales remain unresolved. Figure 6 shows a time series of a volumetric reconstruction of a lifted flame obtained with the same scanning parameters as the one of Fig. 5. The axes of the images are rotated and every second reconstruction is shown ($\Delta t = 1$ ms) to provide a better view of the 3D flame structures and their evolution in time. The closing of a horseshoe-shaped flame structure can be observed and traced in time and space, proving the feasibility of the quasi-4D laser diagnostics using the AOD scanning system. To give a reference of the dimensions, this structure was marked by a circle of 3 mm in diameter at $t = 3$ ms. Detecting these kinds of features is important because

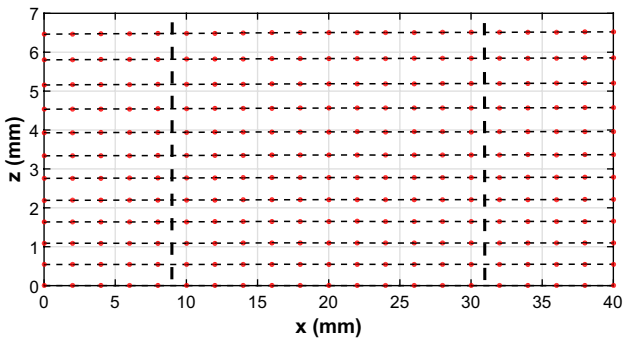

Fig. 4 Parallelization of 12 laser sheets along the x-axis with a scan frequency of 5 kHz and a scan depth of 6.3 mm. The two *vertical dashed lines* mark the measurement volume of the lifted flame experiment

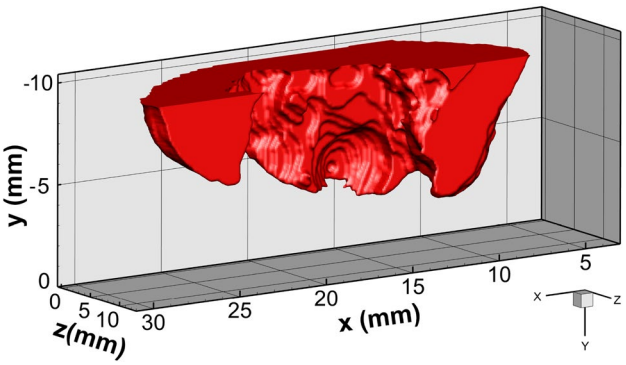

Fig. 5 Volumetric reconstruction snapshot of a lifted flame base from a scan at $f_{scan} = 2$ kHz and 13.7 mm scan depth. Jet and coflow flowing from down to up (negative direction of the y-axis). Laser sheets parallel to the x-axis. View rotated around the y-axis for better visualization of the flame structures. Snapshot smoothed with a $3 \times 3 \times 3$ filter

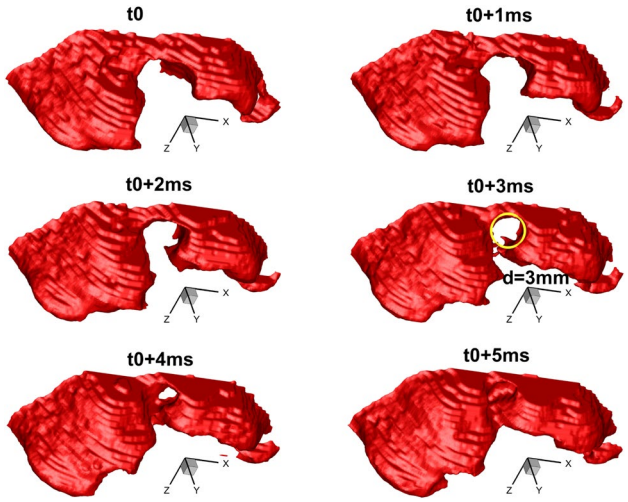

Fig. 6 Time series of a volumetric reconstruction of a lifted flame base from a scan at $f_{scan} = 2$ kHz and 13.7 mm scan depth. Jet and co-flow flowing along the negative direction of the y-axis. Laser sheets parallel to the x-axis. View rotated for better visualization of the flame structures. Snapshot smoothed with a $3 \times 3 \times 3$ filter

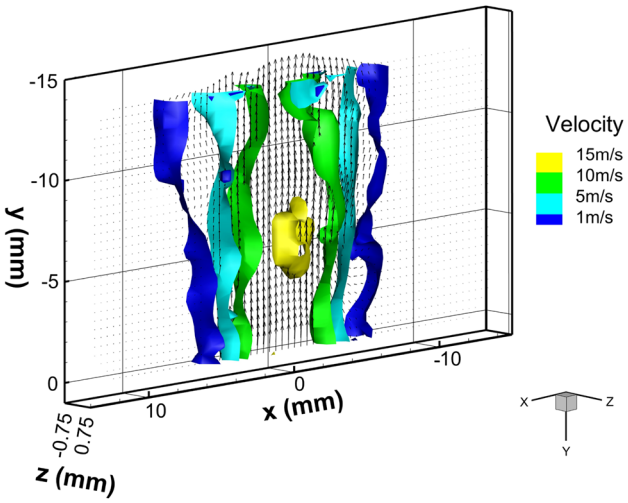

Fig. 7 Example of a velocity field of a non-reacting mixing case measured at three planes with a sheet separation distance of 0.75 mm. Jet and co-flow flowing along the negative direction of the y-axis. Measurement volume centered at $z = 0$ mm

they may not be detected or can be misinterpreted as isolated kernels or unconnected flame structures when using 2D laser techniques [19].

Figure 7 represents a 3D velocity field of a non-reacting mixing reconstructed from the multi-plane 2D PIV measurements. The iso-surfaces of different velocity magnitudes shown in the image are characteristic of a mixing layer of a high-velocity jet propagating into a low-velocity co-flow. Turbulent flow structures, which play an important role when analyzing out-of-plane effects, can be also detected and traced in time and space when using the AOD scanning system.

4 AOD vs. polygonal laser scanning mirror

In a previous work of the authors [12], a polygonal laser scanning mirror (PLSM) was designed and used to perform a quasi-4D visualization of the same lifted turbulent jet flame as presented in this work. This allows a direct comparison of both systems. The custom-made polygon scanner consisted of a 16-facet, 12 mm high, 102 mm in diameter coated aluminum polygon and its motor drive. A cascaded control loop ensured a steady movement and enabled synchronization with an external trigger. The scan angle of 27° was determined by the number of facets, p, and the duty cycle, C, which gives the ratio of the usable area/total area when the laser beams footprint is not cut by the facets edges [13].

$$\Theta = \frac{720 \times C}{p} \tag{3}$$

Any variation of the scan angle requires a rearrangement of the optical setup. The duty cycle was 60% and it corresponded directly to the percentage of usable laser pulses for typical laser operation with an equidistant laser pulse separation. In comparison, the AOD allowed a continuous variation of the scan angle by tuning the input voltage without any changes of the optical setup. The scan angle was within 0–2.3°. The maximum achievable scan angle of the AOD was significantly smaller and every single laser pulse can be used.

The scan frequency f_s of the PLSM is determined by

$$f_s = \frac{p \times n}{60} \tag{4}$$

where n presents the rotational speed of the polygonal mirror. The rotational speed of the brushless DC motor was limited to 40,000 rpm resulting in a maximum scan frequency of 10.67 kHz. Due to aerodynamic losses a helium atmosphere was needed beyond 6.4 kHz. A further increase of the scan frequency can be achieved by (1) increasing the number of facets which in turn decreases the duty cycle if the polygon diameter is kept constant, (2) using more facets with a larger diameter which maintains the duty cycle, but increases mechanical load or (3) increasing the rotational speed which in turn requires higher power devices and is even more critical in terms of safety. For the AOD a scan frequency of 20 kHz was demonstrated within this work. With a laser beam diameter of 6 mm the maximum scan frequency of the AOD is approximately 100 kHz. For smaller beam diameters, scan frequencies beyond 100 kHz

are achievable as long as the damage threshold is not exceeded.

Regarding to the accuracy, the parallelization of the laser path characterized by the deviation angle was 0.14° (scan depth 13.7 mm) for the AOD and 0.6° for the PLSM (scan depth 15 mm). In terms of precision, the jitter of the laser path position was 9 μm independent of the scan frequency for the AOD. For the PLSM the jitter decreases with increasing rpm and was 18 μm for 1 kHz scan frequency and decreased to 9 μm for 5 kHz. Ideally the parameters of the respective controllers are individually adjusted for each scan frequency.

5 Conclusions

A novel scanning system for high-speed quasi-4D laser diagnostics was introduced and characterized. Planar laser measurement techniques were scanned along the third dimension by means of an acousto-optic deflector. In comparison with existing techniques involving mechanical moving parts, the present method reduced the complexity of the optical setup and proved to be very flexible when varying scan parameters such as scan frequency, spatial resolution and the scan depth. Because the AOD can reach scan frequencies beyond 100 kHz, the spatial resolution of the measurement techniques in the direction of the scan can be increased using a faster laser. The stable and precise modulation signal, in combination with a simplified optical setup for parallelization and alignment, allow performing diagnostics such as tomographic imaging and multi-plane PIV with high precision and accuracy of the quasi-volumetric illumination. The present scanning method can be extended to other laser diagnostic techniques such laser-induced fluorescence (LIF). The TeO_2 crystal used in this work is limited to the wavelength range of 350–1600 nm. Other materials (e.g. quartz) are available to extend the wavelength further into the UV range, which could allow using techniques such as OH-LIF. However, those materials are typically characterized by a higher acoustic stiffness, leading to stronger restrictions regarding crystal size and scan angle range.

Acknowledgements The authors gratefully acknowledge the support of Ayane Johchi and Johannes Weinkauff. We also gratefully acknowledge financial support by the Excellence Initiative, Darmstadt Graduate School of Excellence Energy Science and Engineering (GSC 1070) and the Deutsche Forschungsgemeinschaft (DFG, German Research Foundation) through SFB-Transregio 129. Andreas Dreizler is grateful for the generous support by the Gottfried Wilhelm Leibniz program of DFG.

References

1. C. Tropea, A.L. Yarin, J.F. Foss, *Springer Handbook of Experimental Fluid Mechanics* (Springer Science+Business Media, Berlin, 2007), p. 1243
2. I. Boxx, C. Heeger, R. Gordon, B. Böhm, M. Aigner, A. Dreizler, W. Meier, Proc. Combust. Inst. **32**(1), 905–912 (2009)
3. A.M. Steinberg, I. Boxx, C.M. Arndt, J.H. Frank, W. Meier, Proc. Combust. Inst. **33**(1), 1663–1672 (2011)
4. B. Peterson, E. Baum, B. Böhm, A. Dreizler, Proc. Combust. Inst. **35**(3), 3829–3837 (2015)
5. P.J. Trunk, I. Boxx, C. Heeger, W. Meier, B. Böhm, A. Dreizler, Proc. Combust. Inst. **34**(2), 3565–3572 (2013)
6. J. Weinkauff, D. Michaelis, A. Dreizler, B. Böhm, Exp. Fluids **54**, 1624 (2013)
7. C. Atkinson, J. Soria, Exp. Fluids **47**(4–5), 553 (2009)
8. B. Coriton, J.H. Frank, Proc. Combust. Inst. **35**(2), 1243–1250 (2015)
9. J. Weinkauff, J. Köser, D. Michaelis, B. Peterson, A. Dreizler, B. Böhm, in *17th International Symposium on Applications of Laser Techniques to Fluid Mechanics* Lisbon, Portugal (2014)
10. R. Wellander, M. Richter, M. Alden, Exp. Fluids **55**, 1764 (2014)
11. K.Y. Cho, A. Satija, T.L. Pourpoint, S.F. Son, R.P. Lucht, Appl. Opt. **53**(3), 316–326 (2014)
12. J. Weinkauff, M. Greifenstein, A. Dreizler, B. Böhm, Meas. Sci. Technol. **26**(10), 105201 (2015)
13. G.F. Marshall, *Handbook of Optical and Laser Scanning* (Marcel Dekker, New York, 2004), p. 291
14. C. Brücker, Exp. Fluids **19**, 255–263 (1995)
15. G.R.B.E. Römer, P. Bechtold, Phys. Procedia **56**, 2939 (2014)
16. R.G. Hunsperger, *Integrated Optics: Theory and Technology* (Springer, New York, 2009), p. 204
17. I.C. Chang, *Handbook of Optics-Chapter 12* (McGraw-Hill Education, New York, 2010), p. 12.5
18. I.C. Chang, IEEE Trans. Sonics Ultrason. **23**(1), 2–21 (1976)
19. I. Boxx, C. Heeger, R. Gordon, B. Böhm, A. Dreizler, W. Meier, Combust. Flame **156**(1), 269–271 (2009)